

Search for the decay $B^+ \rightarrow \bar{K}^{*0}(892)K^+$

B. Aubert,¹ M. Bona,¹ D. Boutigny,¹ Y. Karyotakis,¹ J. P. Lees,¹ V. Poireau,¹ X. Prudent,¹ V. Tisserand,¹
A. Zghiche,¹ J. Garra Tico,² E. Grauges,² L. Lopez,³ A. Palano,³ G. Eigen,⁴ I. Ofte,⁴ B. Stugu,⁴ L. Sun,⁴
G. S. Abrams,⁵ M. Battaglia,⁵ D. N. Brown,⁵ J. Button-Shafer,⁵ R. N. Cahn,⁵ Y. Groyzman,⁵ R. G. Jacobsen,⁵
J. A. Kadyk,⁵ L. T. Kerth,⁵ Yu. G. Kolomensky,⁵ G. Kukartsev,⁵ D. Lopes Pegna,⁵ G. Lynch,⁵ L. M. Mir,⁵
T. J. Orimoto,⁵ M. Pripstein,⁵ N. A. Roe,⁵ M. T. Ronan,^{5,*} K. Tackmann,⁵ W. A. Wenzel,⁵ P. del Amo Sanchez,⁶
C. M. Hawkes,⁶ A. T. Watson,⁶ T. Held,⁷ H. Koch,⁷ B. Lewandowski,⁷ M. Pelizaeus,⁷ T. Schroeder,⁷ M. Steinke,⁷
J. T. Boyd,⁸ J. P. Burke,⁸ W. N. Cottingham,⁸ D. Walker,⁸ D. J. Asgeirsson,⁹ T. Cuhadar-Donszelmann,⁹
B. G. Fulsom,⁹ C. Hearty,⁹ N. S. Knecht,⁹ T. S. Mattison,⁹ J. A. McKenna,⁹ A. Khan,¹⁰ M. Saleem,¹⁰
L. Teodorescu,¹⁰ V. E. Blinov,¹¹ A. D. Bukin,¹¹ V. P. Druzhinin,¹¹ V. B. Golubev,¹¹ A. P. Onuchin,¹¹
S. I. Serebnyakov,¹¹ Yu. I. Skovpen,¹¹ E. P. Solodov,¹¹ K. Yu Todyshev,¹¹ M. Bondioli,¹² M. Bruinsma,¹² S. Curry,¹²
I. Eschrich,¹² D. Kirkby,¹² A. J. Lankford,¹² P. Lund,¹² M. Mandelkern,¹² E. C. Martin,¹² D. P. Stoker,¹²
S. Abachi,¹³ C. Buchanan,¹³ S. D. Foulkes,¹⁴ J. W. Gary,¹⁴ F. Liu,¹⁴ O. Long,¹⁴ B. C. Shen,¹⁴ L. Zhang,¹⁴
H. P. Paar,¹⁵ S. Rahatlou,¹⁵ V. Sharma,¹⁵ J. W. Berryhill,¹⁶ C. Campagnari,¹⁶ A. Cunha,¹⁶ B. Dahmes,¹⁶
T. M. Hong,¹⁶ D. Kovalskyi,¹⁶ J. D. Richman,¹⁶ T. W. Beck,¹⁷ A. M. Eisner,¹⁷ C. J. Flacco,¹⁷ C. A. Heusch,¹⁷
J. Kroseberg,¹⁷ W. S. Lockman,¹⁷ T. Schalk,¹⁷ B. A. Schumm,¹⁷ A. Seiden,¹⁷ D. C. Williams,¹⁷ M. G. Wilson,¹⁷
L. O. Winstrom,¹⁷ E. Chen,¹⁸ C. H. Cheng,¹⁸ A. Dvoretzki,¹⁸ F. Fang,¹⁸ D. G. Hitlin,¹⁸ I. Narsky,¹⁸ T. Piatenko,¹⁸
F. C. Porter,¹⁸ G. Mancinelli,¹⁹ B. T. Meadows,¹⁹ K. Mishra,¹⁹ M. D. Sokoloff,¹⁹ F. Blanc,²⁰ P. C. Bloom,²⁰
S. Chen,²⁰ W. T. Ford,²⁰ J. F. Hirschauer,²⁰ A. Kreisel,²⁰ M. Nagel,²⁰ U. Nauenberg,²⁰ A. Olivas,²⁰ J. G. Smith,²⁰
K. A. Ulmer,²⁰ S. R. Wagner,²⁰ J. Zhang,²⁰ A. Chen,²¹ E. A. Eckhart,²¹ A. Soffer,²¹ W. H. Toki,²¹ R. J. Wilson,²¹
F. Winklmeier,²¹ Q. Zeng,²¹ D. D. Altenburg,²² E. Feltresi,²² A. Hauke,²² H. Jasper,²² J. Merkel,²² A. Petzold,²²
B. Spaan,²² K. Wacker,²² T. Brandt,²³ V. Klose,²³ H. M. Lacker,²³ W. F. Mader,²³ R. Nogowski,²³ J. Schubert,²³
K. R. Schubert,²³ R. Schwierz,²³ J. E. Sundermann,²³ A. Volk,²³ D. Bernard,²⁴ G. R. Bonneaud,²⁴ E. Latour,²⁴
Ch. Thiebaux,²⁴ M. Verderi,²⁴ P. J. Clark,²⁵ W. Gradl,²⁵ F. Muheim,²⁵ S. Playfer,²⁵ A. I. Robertson,²⁵ Y. Xie,²⁵
M. Andreotti,²⁶ D. Bettoni,²⁶ C. Bozzi,²⁶ R. Calabrese,²⁶ A. Cecchi,²⁶ G. Cibinetto,²⁶ P. Franchini,²⁶ E. Luppi,²⁶
M. Negrini,²⁶ A. Petrella,²⁶ L. Piemontese,²⁶ E. Prencipe,²⁶ V. Santoro,²⁶ F. Anulli,²⁷ R. Baldini-Ferroli,²⁷
A. Calcaterra,²⁷ R. de Sangro,²⁷ G. Finocchiaro,²⁷ S. Pacetti,²⁷ P. Patteri,²⁷ I. M. Peruzzi,²⁷ † M. Piccolo,²⁷
M. Rama,²⁷ A. Zallo,²⁷ A. Buzzo,²⁸ R. Contri,²⁸ M. Lo Vetere,²⁸ M. M. Macri,²⁸ M. R. Monge,²⁸ S. Passaggio,²⁸
C. Patrignani,²⁸ E. Robutti,²⁸ A. Santroni,²⁸ S. Tosi,²⁸ K. S. Chaisanguanthum,²⁹ M. Morii,²⁹ J. Wu,²⁹
R. S. Dubitzky,³⁰ J. Marks,³⁰ S. Schenk,³⁰ U. Uwer,³⁰ D. J. Bard,³¹ P. D. Dauncey,³¹ R. L. Flack,³¹ J. A. Nash,³¹
M. B. Nikolich,³¹ W. Panduro Vazquez,³¹ P. K. Behera,³² X. Chai,³² M. J. Charles,³² U. Mallik,³² N. T. Meyer,³²
V. Ziegler,³² J. Cochran,³³ H. B. Crawley,³³ L. Dong,³³ V. Eyges,³³ W. T. Meyer,³³ S. Prell,³³ E. I. Rosenberg,³³
A. E. Rubin,³³ A. V. Gritsan,³⁴ C. K. Lae,³⁴ A. G. Denig,³⁵ M. Fritsch,³⁵ G. Schott,³⁵ N. Arnaud,³⁶
J. Béquilleux,³⁶ M. Davier,³⁶ G. Grosdidier,³⁶ A. Höcker,³⁶ V. Lepeltier,³⁶ F. Le Diberder,³⁶ A. M. Lutz,³⁶
S. Pruvot,³⁶ S. Rodier,³⁶ P. Roudeau,³⁶ M. H. Schune,³⁶ J. Serrano,³⁶ V. Sordini,³⁶ A. Stocchi,³⁶ W. F. Wang,³⁶
G. Wormser,³⁶ D. J. Lange,³⁷ D. M. Wright,³⁷ C. A. Chavez,³⁸ I. J. Forster,³⁸ J. R. Fry,³⁸ E. Gabathuler,³⁸
R. Gamet,³⁸ D. E. Hutchcroft,³⁸ D. J. Payne,³⁸ K. C. Schofield,³⁸ C. Touramanis,³⁸ A. J. Bevan,³⁹ K. A. George,³⁹
F. Di Lodovico,³⁹ W. Menges,³⁹ R. Sacco,³⁹ G. Cowan,⁴⁰ H. U. Flaecher,⁴⁰ D. A. Hopkins,⁴⁰ P. S. Jackson,⁴⁰
T. R. McMahon,⁴⁰ F. Salvatore,⁴⁰ A. C. Wren,⁴⁰ D. N. Brown,⁴¹ C. L. Davis,⁴¹ J. Allison,⁴² N. R. Barlow,⁴²
R. J. Barlow,⁴² Y. M. Chia,⁴² C. L. Edgar,⁴² G. D. Lafferty,⁴² T. J. West,⁴² J. I. Yi,⁴² J. Anderson,⁴³ C. Chen,⁴³
A. Jawahery,⁴³ D. A. Roberts,⁴³ G. Simi,⁴³ J. M. Tuggle,⁴³ G. Blaylock,⁴⁴ C. Dallapiccola,⁴⁴ S. S. Hertzbach,⁴⁴
X. Li,⁴⁴ T. B. Moore,⁴⁴ E. Salvati,⁴⁴ S. Saremi,⁴⁴ R. Cowan,⁴⁵ P. H. Fisher,⁴⁵ G. Sciolla,⁴⁵ S. J. Sekula,⁴⁵
M. Spitznagel,⁴⁵ F. Taylor,⁴⁵ R. K. Yamamoto,⁴⁵ H. Kim,⁴⁶ S. E. Mclachlin,⁴⁶ P. M. Patel,⁴⁶ S. H. Robertson,⁴⁶
A. Lazzaro,⁴⁷ V. Lombardo,⁴⁷ F. Palombo,⁴⁷ J. M. Bauer,⁴⁸ L. Cremaldi,⁴⁸ V. Eschenburg,⁴⁸ R. Godang,⁴⁸
R. Kroeger,⁴⁸ D. A. Sanders,⁴⁸ D. J. Summers,⁴⁸ H. W. Zhao,⁴⁸ S. Brunet,⁴⁹ D. Côté,⁴⁹ M. Simard,⁴⁹ P. Taras,⁴⁹
F. B. Viaud,⁴⁹ H. Nicholson,⁵⁰ G. De Nardo,⁵¹ F. Fabozzi,⁵¹ ‡ L. Lista,⁵¹ D. Monorchio,⁵¹ C. Sciacca,⁵¹
M. A. Baak,⁵² G. Raven,⁵² H. L. Snoek,⁵² C. P. Jessop,⁵³ J. M. LoSecco,⁵³ G. Benelli,⁵⁴ L. A. Corwin,⁵⁴
K. K. Gan,⁵⁴ K. Honscheid,⁵⁴ D. Hufnagel,⁵⁴ H. Kagan,⁵⁴ R. Kass,⁵⁴ J. P. Morris,⁵⁴ A. M. Rahimi,⁵⁴
J. J. Regensburger,⁵⁴ R. Ter-Antonyan,⁵⁴ Q. K. Wong,⁵⁴ N. L. Blount,⁵⁵ J. Brau,⁵⁵ R. Frey,⁵⁵ O. Igonkina,⁵⁵

J. A. Kolb,⁵⁵ M. Lu,⁵⁵ R. Rahmat,⁵⁵ N. B. Sinev,⁵⁵ D. Strom,⁵⁵ J. Strube,⁵⁵ E. Torrence,⁵⁵ N. Gagliardi,⁵⁶ A. Gaz,⁵⁶ M. Margoni,⁵⁶ M. Morandin,⁵⁶ A. Pompili,⁵⁶ M. Posocco,⁵⁶ M. Rotondo,⁵⁶ F. Simonetto,⁵⁶ R. Stroili,⁵⁶ C. Voci,⁵⁶ E. Ben-Haim,⁵⁷ H. Briand,⁵⁷ J. Chauveau,⁵⁷ P. David,⁵⁷ L. Del Buono,⁵⁷ Ch. de la Vaissière,⁵⁷ O. Hamon,⁵⁷ B. L. Hartfiel,⁵⁷ Ph. Leruste,⁵⁷ J. Malcès,⁵⁷ J. Ocariz,⁵⁷ A. Perez,⁵⁷ L. Gladney,⁵⁸ M. Biasini,⁵⁹ R. Covarelli,⁵⁹ E. Manoni,⁵⁹ C. Angelini,⁶⁰ G. Batignani,⁶⁰ S. Bettarini,⁶⁰ G. Calderini,⁶⁰ M. Carpinelli,⁶⁰ R. Cenci,⁶⁰ F. Forti,⁶⁰ M. A. Giorgi,⁶⁰ A. Lusiani,⁶⁰ G. Marchiori,⁶⁰ M. A. Mazur,⁶⁰ M. Morganti,⁶⁰ N. Neri,⁶⁰ E. Paoloni,⁶⁰ G. Rizzo,⁶⁰ J. J. Walsh,⁶⁰ M. Haire,⁶¹ J. Biesiada,⁶² P. Elmer,⁶² Y. P. Lau,⁶² C. Lu,⁶² J. Olsen,⁶² A. J. S. Smith,⁶² A. V. Telnov,⁶² E. Baracchini,⁶³ F. Bellini,⁶³ G. Cavoto,⁶³ A. D’Orazio,⁶³ D. del Re,⁶³ E. Di Marco,⁶³ R. Faccini,⁶³ F. Ferrarotto,⁶³ F. Ferroni,⁶³ M. Gaspero,⁶³ P. D. Jackson,⁶³ L. Li Gioi,⁶³ M. A. Mazzoni,⁶³ S. Morganti,⁶³ G. Piredda,⁶³ F. Polci,⁶³ F. Renga,⁶³ C. Voena,⁶³ M. Ebert,⁶⁴ H. Schröder,⁶⁴ R. Waldi,⁶⁴ T. Adye,⁶⁵ G. Castelli,⁶⁵ B. Franek,⁶⁵ E. O. Olaiya,⁶⁵ S. Ricciardi,⁶⁵ W. Roethel,⁶⁵ F. F. Wilson,⁶⁵ R. Aleksan,⁶⁶ S. Emery,⁶⁶ M. Escalier,⁶⁶ A. Gaidot,⁶⁶ S. F. Ganzhur,⁶⁶ G. Hamel de Monchenault,⁶⁶ W. Kozanecki,⁶⁶ M. Legendre,⁶⁶ G. Vasseur,⁶⁶ Ch. Yèche,⁶⁶ M. Zito,⁶⁶ X. R. Chen,⁶⁷ H. Liu,⁶⁷ W. Park,⁶⁷ M. V. Purohit,⁶⁷ J. R. Wilson,⁶⁷ M. T. Allen,⁶⁸ D. Aston,⁶⁸ R. Bartoldus,⁶⁸ P. Bechtle,⁶⁸ N. Berger,⁶⁸ R. Claus,⁶⁸ J. P. Coleman,⁶⁸ M. R. Convery,⁶⁸ J. C. Dingfelder,⁶⁸ J. Dorfan,⁶⁸ G. P. Dubois-Felsmann,⁶⁸ D. Dujmic,⁶⁸ W. Dunwoodie,⁶⁸ R. C. Field,⁶⁸ T. Glanzman,⁶⁸ S. J. Gowdy,⁶⁸ M. T. Graham,⁶⁸ P. Grenier,⁶⁸ V. Halyo,⁶⁸ C. Hast,⁶⁸ T. Hryn’ova,⁶⁸ W. R. Innes,⁶⁸ M. H. Kelsey,⁶⁸ P. Kim,⁶⁸ D. W. G. S. Leith,⁶⁸ S. Li,⁶⁸ S. Luitz,⁶⁸ V. Luth,⁶⁸ H. L. Lynch,⁶⁸ D. B. MacFarlane,⁶⁸ H. Marsiske,⁶⁸ R. Messner,⁶⁸ D. R. Muller,⁶⁸ C. P. O’Grady,⁶⁸ V. E. Ozcan,⁶⁸ A. Perazzo,⁶⁸ M. Perl,⁶⁸ T. Pulliam,⁶⁸ B. N. Ratcliff,⁶⁸ A. Roodman,⁶⁸ A. A. Salnikov,⁶⁸ R. H. Schindler,⁶⁸ J. Schwiening,⁶⁸ A. Snyder,⁶⁸ J. Stelzer,⁶⁸ D. Su,⁶⁸ M. K. Sullivan,⁶⁸ K. Suzuki,⁶⁸ S. K. Swain,⁶⁸ J. M. Thompson,⁶⁸ J. Va’vra,⁶⁸ N. van Bakel,⁶⁸ A. P. Wagner,⁶⁸ M. Weaver,⁶⁸ W. J. Wisniewski,⁶⁸ M. Wittgen,⁶⁸ D. H. Wright,⁶⁸ A. K. Yarritu,⁶⁸ K. Yi,⁶⁸ C. C. Young,⁶⁸ P. R. Burchat,⁶⁹ A. J. Edwards,⁶⁹ S. A. Majewski,⁶⁹ B. A. Petersen,⁶⁹ L. Wilden,⁶⁹ S. Ahmed,⁷⁰ M. S. Alam,⁷⁰ R. Bula,⁷⁰ J. A. Ernst,⁷⁰ V. Jain,⁷⁰ B. Pan,⁷⁰ M. A. Saeed,⁷⁰ F. R. Wappler,⁷⁰ S. B. Zain,⁷⁰ W. Bugg,⁷¹ M. Krishnamurthy,⁷¹ S. M. Spanier,⁷¹ R. Eckmann,⁷² J. L. Ritchie,⁷² A. M. Ruland,⁷² C. J. Schilling,⁷² R. F. Schwitters,⁷² J. M. Izen,⁷³ X. C. Lou,⁷³ S. Ye,⁷³ F. Bianchi,⁷⁴ F. Gallo,⁷⁴ D. Gamba,⁷⁴ M. Pelliccioni,⁷⁴ M. Bomben,⁷⁵ L. Bosisio,⁷⁵ C. Cartaro,⁷⁵ F. Cossutti,⁷⁵ G. Della Ricca,⁷⁵ L. Lanceri,⁷⁵ L. Vitale,⁷⁵ V. Azzolini,⁷⁶ N. Lopez-March,⁷⁶ F. Martinez-Vidal,⁷⁶ D. A. Milanese,⁷⁶ A. Oyanguren,⁷⁶ J. Albert,⁷⁷ Sw. Banerjee,⁷⁷ B. Bhuyan,⁷⁷ K. Hamano,⁷⁷ R. Kowalewski,⁷⁷ I. M. Nugent,⁷⁷ J. M. Roney,⁷⁷ R. J. Sobie,⁷⁷ J. J. Back,⁷⁸ P. F. Harrison,⁷⁸ T. E. Latham,⁷⁸ G. B. Mohanty,⁷⁸ M. Pappagallo,^{78,§} H. R. Band,⁷⁹ X. Chen,⁷⁹ S. Dasu,⁷⁹ K. T. Flood,⁷⁹ J. J. Hollar,⁷⁹ P. E. Kutter,⁷⁹ Y. Pan,⁷⁹ M. Pierini,⁷⁹ R. Prepost,⁷⁹ S. L. Wu,⁷⁹ Z. Yu,⁷⁹ and H. Neal⁸⁰

(The BABAR Collaboration)

¹Laboratoire de Physique des Particules, IN2P3/CNRS et Université de Savoie, F-74941 Annecy-Le-Vieux, France

²Universitat de Barcelona, Facultat de Física, Departament ECM, E-08028 Barcelona, Spain

³Università di Bari, Dipartimento di Fisica and INFN, I-70126 Bari, Italy

⁴University of Bergen, Institute of Physics, N-5007 Bergen, Norway

⁵Lawrence Berkeley National Laboratory and University of California, Berkeley, California 94720, USA

⁶University of Birmingham, Birmingham, B15 2TT, United Kingdom

⁷Ruhr Universität Bochum, Institut für Experimentalphysik 1, D-44780 Bochum, Germany

⁸University of Bristol, Bristol BS8 1TL, United Kingdom

⁹University of British Columbia, Vancouver, British Columbia, Canada V6T 1Z1

¹⁰Brunel University, Uxbridge, Middlesex UB8 3PH, United Kingdom

¹¹Budker Institute of Nuclear Physics, Novosibirsk 630090, Russia

¹²University of California at Irvine, Irvine, California 92697, USA

¹³University of California at Los Angeles, Los Angeles, California 90024, USA

¹⁴University of California at Riverside, Riverside, California 92521, USA

¹⁵University of California at San Diego, La Jolla, California 92093, USA

¹⁶University of California at Santa Barbara, Santa Barbara, California 93106, USA

¹⁷University of California at Santa Cruz, Institute for Particle Physics, Santa Cruz, California 95064, USA

¹⁸California Institute of Technology, Pasadena, California 91125, USA

¹⁹University of Cincinnati, Cincinnati, Ohio 45221, USA

²⁰University of Colorado, Boulder, Colorado 80309, USA

²¹Colorado State University, Fort Collins, Colorado 80523, USA

²²Universität Dortmund, Institut für Physik, D-44221 Dortmund, Germany

²³Technische Universität Dresden, Institut für Kern- und Teilchenphysik, D-01062 Dresden, Germany

²⁴Laboratoire Leprince-Ringuet, CNRS/IN2P3, Ecole Polytechnique, F-91128 Palaiseau, France

²⁵University of Edinburgh, Edinburgh EH9 3JZ, United Kingdom

²⁶Università di Ferrara, Dipartimento di Fisica and INFN, I-44100 Ferrara, Italy

- ²⁷Laboratori Nazionali di Frascati dell'INFN, I-00044 Frascati, Italy
- ²⁸Università di Genova, Dipartimento di Fisica and INFN, I-16146 Genova, Italy
- ²⁹Harvard University, Cambridge, Massachusetts 02138, USA
- ³⁰Universität Heidelberg, Physikalisches Institut, Philosophenweg 12, D-69120 Heidelberg, Germany
- ³¹Imperial College London, London, SW7 2AZ, United Kingdom
- ³²University of Iowa, Iowa City, Iowa 52242, USA
- ³³Iowa State University, Ames, Iowa 50011-3160, USA
- ³⁴Johns Hopkins University, Baltimore, Maryland 21218, USA
- ³⁵Universität Karlsruhe, Institut für Experimentelle Kernphysik, D-76021 Karlsruhe, Germany
- ³⁶Laboratoire de l'Accélérateur Linéaire, IN2P3/CNRS et Université Paris-Sud 11, Centre Scientifique d'Orsay, B. P. 34, F-91898 ORSAY Cedex, France
- ³⁷Lawrence Livermore National Laboratory, Livermore, California 94550, USA
- ³⁸University of Liverpool, Liverpool L69 7ZE, United Kingdom
- ³⁹Queen Mary, University of London, E1 4NS, United Kingdom
- ⁴⁰University of London, Royal Holloway and Bedford New College, Egham, Surrey TW20 0EX, United Kingdom
- ⁴¹University of Louisville, Louisville, Kentucky 40292, USA
- ⁴²University of Manchester, Manchester M13 9PL, United Kingdom
- ⁴³University of Maryland, College Park, Maryland 20742, USA
- ⁴⁴University of Massachusetts, Amherst, Massachusetts 01003, USA
- ⁴⁵Massachusetts Institute of Technology, Laboratory for Nuclear Science, Cambridge, Massachusetts 02139, USA
- ⁴⁶McGill University, Montréal, Québec, Canada H3A 2T8
- ⁴⁷Università di Milano, Dipartimento di Fisica and INFN, I-20133 Milano, Italy
- ⁴⁸University of Mississippi, University, Mississippi 38677, USA
- ⁴⁹Université de Montréal, Physique des Particules, Montréal, Québec, Canada H3C 3J7
- ⁵⁰Mount Holyoke College, South Hadley, Massachusetts 01075, USA
- ⁵¹Università di Napoli Federico II, Dipartimento di Scienze Fisiche and INFN, I-80126, Napoli, Italy
- ⁵²NIKHEF, National Institute for Nuclear Physics and High Energy Physics, NL-1009 DB Amsterdam, The Netherlands
- ⁵³University of Notre Dame, Notre Dame, Indiana 46556, USA
- ⁵⁴Ohio State University, Columbus, Ohio 43210, USA
- ⁵⁵University of Oregon, Eugene, Oregon 97403, USA
- ⁵⁶Università di Padova, Dipartimento di Fisica and INFN, I-35131 Padova, Italy
- ⁵⁷Laboratoire de Physique Nucléaire et de Hautes Energies, IN2P3/CNRS, Université Pierre et Marie Curie-Paris6, Université Denis Diderot-Paris7, F-75252 Paris, France
- ⁵⁸University of Pennsylvania, Philadelphia, Pennsylvania 19104, USA
- ⁵⁹Università di Perugia, Dipartimento di Fisica and INFN, I-06100 Perugia, Italy
- ⁶⁰Università di Pisa, Dipartimento di Fisica, Scuola Normale Superiore and INFN, I-56127 Pisa, Italy
- ⁶¹Prairie View A&M University, Prairie View, Texas 77446, USA
- ⁶²Princeton University, Princeton, New Jersey 08544, USA
- ⁶³Università di Roma La Sapienza, Dipartimento di Fisica and INFN, I-00185 Roma, Italy
- ⁶⁴Universität Rostock, D-18051 Rostock, Germany
- ⁶⁵Rutherford Appleton Laboratory, Chilton, Didcot, Oxon, OX11 0QX, United Kingdom
- ⁶⁶DSM/Dapnia, CEA/Saclay, F-91191 Gif-sur-Yvette, France
- ⁶⁷University of South Carolina, Columbia, South Carolina 29208, USA
- ⁶⁸Stanford Linear Accelerator Center, Stanford, California 94309, USA
- ⁶⁹Stanford University, Stanford, California 94305-4060, USA
- ⁷⁰State University of New York, Albany, New York 12222, USA
- ⁷¹University of Tennessee, Knoxville, Tennessee 37996, USA
- ⁷²University of Texas at Austin, Austin, Texas 78712, USA
- ⁷³University of Texas at Dallas, Richardson, Texas 75083, USA
- ⁷⁴Università di Torino, Dipartimento di Fisica Sperimentale and INFN, I-10125 Torino, Italy
- ⁷⁵Università di Trieste, Dipartimento di Fisica and INFN, I-34127 Trieste, Italy
- ⁷⁶IFIC, Universitat de Valencia-CSIC, E-46071 Valencia, Spain
- ⁷⁷University of Victoria, Victoria, British Columbia, Canada V8W 3P6
- ⁷⁸Department of Physics, University of Warwick, Coventry CV4 7AL, United Kingdom
- ⁷⁹University of Wisconsin, Madison, Wisconsin 53706, USA
- ⁸⁰Yale University, New Haven, Connecticut 06511, USA

(Dated: November 27, 2007)

We report on a search for the process $B^+ \rightarrow \bar{K}^{*0}(892)K^+$ using $232 \times 10^6 \Upsilon(4S) \rightarrow B\bar{B}$ decays collected with the BABAR detector at the PEP-II asymmetric-energy B Factory at SLAC. From a signal yield of $25 \pm 13 [\text{stat}] \pm 7 [\text{syst}] B^+ \rightarrow \bar{K}^{*0}(892)(\rightarrow K^-\pi^+)K^+$ events, we place an upper limit on the branching fraction $\mathcal{B}(B^+ \rightarrow \bar{K}^{*0}(892)K^+)$ of 1.1×10^{-6} , at the 90% confidence level.

We present a measurement of the branching fraction $\mathcal{B}(B^+ \rightarrow \bar{K}^{*0}(892)K^+)$ based exclusively on B^+ decays to the final state $K^+K^-\pi^+$. Charge conjugate states are assumed throughout. In the Standard Model (SM), $B \rightarrow K^*K$ decays are dominated by $b \rightarrow ds\bar{s}$ gluonic penguin diagrams (see Figure 1(a) in [1]; for the charged decay the spectator \bar{d} is replaced with \bar{u}). Such transitions provide a valuable tool with which to test the quark-flavor sector of the SM (see, for example, [2–4]). The mode $B^+ \rightarrow \bar{K}^{*0}(892)K^+$ is also relevant for the interpretation of the time dependent CP asymmetry obtained with the $B^0 \rightarrow \phi K_s^0$ mode. To leading order the CP asymmetry equals $\sin 2\beta$ for this mode, where β is the Unitarity Triangle (UT) angle. However, sub-dominant amplitudes proportional to $V_{ub}^*V_{us}$ could produce a deviation $\Delta S_{\phi K_s^0}$ from $\sin 2\beta$. Exploiting SU(3) flavor symmetry and combining measured rates for relevant $b \rightarrow s$ and $b \rightarrow d$ processes (including $B^+ \rightarrow \bar{K}^{*0}(892)K^+$), a method is introduced in [5] to place a bound on $\Delta S_{\phi K_s^0}$. Measurements yielding a significant deviation in excess of such a bound would be a strong indication of physics beyond the SM. Furthermore, $B^+ \rightarrow \bar{K}^{*0}(892)K^+$ is one of several charmless decays that can be used, together with U-spin symmetry, to extract the UT angle γ [6].

Theoretical predictions for $\mathcal{B}(B^+ \rightarrow \bar{K}^{*0}(892)K^+)$ include $\mathcal{B}(B^+ \rightarrow \bar{K}^{*0}(892)K^+) > (0.46_{-0.07}^{+0.06}) \times 10^{-6}$ [2] and $\mathcal{B}(B^+ \rightarrow \bar{K}^{*0}(892)K^+) \approx 0.5 \times 10^{-6}$ [3]—both using SU(3) flavor symmetry and experimental information for charmless B decays, and $\mathcal{B}(B^+ \rightarrow \bar{K}^{*0}(892)K^+) \approx 0.31 \times 10^{-6}$ —using perturbative QCD factorization [4]. Prior to the analysis presented here, the only experimental limit placed on $\mathcal{B}(B^+ \rightarrow \bar{K}^{*0}(892)K^+)$ was that presented by the CLEO collaboration at the 90% confidence level (CL) [7]: $\mathcal{B}(B^+ \rightarrow \bar{K}^{*0}(892)K^+) < 5.3 \times 10^{-6}$.

The data used in this analysis were collected with the BABAR detector [8] at the PEP-II asymmetric-energy e^+e^- storage ring at the Stanford Linear Accelerator Center. Charged particle trajectories are measured by a five-layer double-sided silicon vertex tracker and a 40-layer drift chamber located within a 1.5 T axial magnetic field. Charged hadrons are identified by combining energy loss information from tracking (dE/dx) with the measurements from a ring-imaging Cherenkov detector. Photons and electrons are detected by a CsI(Tl) crystal electromagnetic calorimeter. The magnet’s flux return is instrumented for muon and neutral hadron identification.

The data sample consists of $(232 \pm 3) \times 10^6$ $B\bar{B}$ pairs

collected at the $\Upsilon(4S)$ resonance (on-resonance data), corresponding to an integrated luminosity of 211 fb^{-1} . It is assumed that neutral and charged B meson pairs are produced in equal numbers [9]. In addition, 22 fb^{-1} of data collected 40 MeV below the $\Upsilon(4S)$ resonance (off-resonance data) are used for background studies.

B meson candidates are reconstructed from three charged tracks. The charged tracks are required to have at least 12 hits in the drift chamber and a transverse momentum greater than $0.1 \text{ GeV}/c$. They are fitted to a common vertex; momentum must be conserved at this vertex. Two of the tracks must have opposite charge and a signal in the tracking and Cherenkov detectors that is consistent with that of a kaon. We remove tracks that pass electron selection criteria based on dE/dx and calorimeter information.

We perform full detector Monte Carlo (MC) simulations equivalent to 2.4×10^5 signal $B^+ \rightarrow \bar{K}^{*0}(892)(\rightarrow K^-\pi^+)K^+$ decays. For background studies 1.0 ab^{-1} of generic $B\bar{B}$ decays are simulated, as are over 100 exclusive B meson decay modes ($\sim 10^4 - 10^6$ events/mode), approximately half of which are charmless. MC samples are generated with EvtGen [10], while the detector response is simulated with GEANT4 [11]. All simulated events are reconstructed in the same manner as data. Off-resonance data are used to measure the properties of the light quark continuum decays, $e^+e^- \rightarrow q\bar{q}$ ($q = u, d, s, c$).

For correctly reconstructed signal events, $\Delta E = E_B^* - \sqrt{s}/2$ peaks at zero, while $m_{ES} = \sqrt{(s/2 + \mathbf{p}_0 \cdot \mathbf{p}_B)^2/E_0^2 - \mathbf{p}_B^2}$ peaks at the B mass. The resolutions of these largely uncorrelated kinematic variables, for signal events, are $\approx 20 \text{ MeV}$ and $\approx 2.5 \text{ MeV}/c^2$, respectively. E_B^* is the B meson candidate energy in the center-of-mass (CM) frame, E_0 and \sqrt{s} are the total energies of the e^+e^- system in the laboratory and CM frames, respectively, and \mathbf{p}_0 and \mathbf{p}_B are the three-momenta of the e^+e^- system and the B meson candidate in the laboratory frame. The distributions for continuum events are slowly varying. For B meson decays in which particle misidentification occurs, the ΔE peak is shifted by 500 or more MeV. Events are selected with $5.22 < m_{ES} < 5.29 \text{ GeV}/c^2$ and $|\Delta E| < 0.1 \text{ GeV}$. The ΔE restriction helps to remove background from two- and four-body B meson decays at a small cost to signal efficiency.

Continuum quark-antiquark production is the dominant background. To suppress it, we select only those events where the angle θ_T in the CM frame between the thrust axis of the B meson candidate and the thrust axis of the rest of the event satisfies $|\cos \theta_T| < 0.9$. For continuum events, which tend to be jet-like in the CM frame, the distribution of $|\cos \theta_T|$ is strongly peaked toward unity whereas the distribution is uniform for signal events in which little kinetic energy is available in

*Deceased

†Also with Università di Perugia, Dipartimento di Fisica, Perugia, Italy

‡Also with Università della Basilicata, Potenza, Italy

§Also with IPPP, Physics Department, Durham University, Durham DH1 3LE, United Kingdom

the CM frame. The number of continuum background events present per signal event is reduced by a factor of approximately two with the application of the $|\cos\theta_T|$ cut. We also construct a Fisher discriminant [12] \mathcal{F} , a linear combination of five variables: the zeroth and second angular moments of the energy flow—excluding the B candidate—about the B thrust axis; the absolute value of the cosine of the angle between the momentum vector of the reconstructed B candidate and the beam direction; the absolute value of the cosine of the angle between the thrust axis of the reconstructed B candidate and the beam direction; and the output of a multivariate, non-linear B meson candidate flavor tagging algorithm [13]. The Fisher coefficients are obtained from samples of off-resonance data and $B^+ \rightarrow K^+K^-\pi^+$ MC. A loose cut of $|\mathcal{F}| < 3.0$ is applied. This cut eliminates a negligible fraction of signal and background events and is applied only to define a range for the fit (see below).

Further discrimination between signal and continuum background is achieved by utilizing the variables $m_{K\pi}$ and $\cos\theta_H$. The invariant mass of the $\bar{K}^{*0}(892)$ candidate, $m_{K\pi}$, is restricted to $0.744 < m_{K\pi} < 1.048 \text{ GeV}/c^2$. We also require that the cosine of the helicity angle, θ_H , is less than 0.9, where θ_H is defined to be the angle between the pion track and the spectator kaon track in the rest frame of the $\bar{K}^{*0}(892)$. This angle depends on the spin of the intermediate resonance: for $B^+ \rightarrow K^+K^-\pi^+$ via the spin-1 $\bar{K}^{*0}(892)$ resonance, the distribution of its cosine is quadratic. For continuum events the distribution is approximately uniform. At high $\cos\theta_H$ the final state pion has low momentum and is difficult to reconstruct. This causes a sharp drop-off in the efficiency between 0.9 and 1.0. The selection criterion $\cos\theta_H < 0.9$ makes an unbinned fit to the variable possible at a cost of losing 5% of signal events.

After the selection described above, the $B^+ \rightarrow \bar{K}^{*0}(892)(\rightarrow K^-\pi^+)K^+$ selection efficiency is 26%. In signal MC studies, the signal candidate is correctly reconstructed 94% of the time. The remaining candidates come from self-cross-feed (SCF) events that stem from swapping one or more tracks from the true B meson decay with tracks from the rest of the event.

To identify backgrounds from B meson decays the selection criteria described above are applied to the MC samples. Using the efficiencies of the selection criteria and world average branching fractions we find that the largest expected contributions derive from $b \rightarrow c$ transitions and from charmless 3-body decays in which a kaon is misidentified as a pion or vice versa. The $b \rightarrow c$ events, combinatoric in nature, are continuum-like in most of the fit variables. As such, the contribution to the fitted signal is small: $\sim 1\%$ of the number of $b \rightarrow c$ events expected to be present. For charmless 3-body sources, however, the contribution to the signal yield—as a proportion of the number of events present—is considerably larger. This is particularly true of $B^+ \rightarrow K^+K^-K^+$ and $B^+ \rightarrow \rho K^+$. The decay $B^+ \rightarrow K^+K^-K^+$ includes non-resonant and several intermediate resonance states, in-

cluding the narrow ϕ state. In order to increase statistical precision, ϕK^+ is considered separately from the rest of the $K^+K^-K^+$ final state, which is modeled using the results of the Dalitz plot analysis in [14]. Since the ϕ is very narrow, its interference with the other $K^+K^-K^+$ states can be neglected in this context. The modes $B^+ \rightarrow \phi K^+$, $B^+ \rightarrow K^+K^-K^+$, and $B^+ \rightarrow \rho K^+$, are therefore included as components of the fit. This eliminates biases on the fitted signal yield due to these channels.

The contribution to the signal yield due to all other sources of B meson background (including the $b \rightarrow c$ modes discussed above and numerous charmless modes) is estimated from simulation at 3 events—to which a conservative $\pm 100\%$ uncertainty is assigned. The uncertainty accounts for poorly known branching fractions and simulation limitations. Individually these sources contribute at a low level. As such, rather than including components for each of them in the fit, a correction to the fitted signal yield is made.

It is also necessary to consider backgrounds from B meson decays that have the same final state as the signal mode. MC studies of the $B^+ \rightarrow K^+K^-\pi^+$ Dalitz plot show that the only contribution that needs to be accounted for is $B^+ \rightarrow \bar{K}_0^{*0}(1430)(\rightarrow K^-\pi^+)K^+$. We use the LASS parameterization for the $\bar{K}_0^{*0}(1430)$ lineshape, which consists of the $\bar{K}_0^{*0}(1430)$ resonance together with an effective range non-resonant component [15]. We take $\mathcal{B}(\bar{K}_0^{*0}(1430) \rightarrow K^-\pi^+)$ to be equal to $\frac{2}{3} \times (93 \pm 10)\%$ [16]. A maximum likelihood fit to three variables— m_{ES} , ΔE , and \mathcal{F} —is performed in a region of the $K^-\pi^+$ invariant mass spectrum between 1.048 and 1.800 GeV/c^2 in an analogous way to how we fit the main signal (see below). A 90% CL upper limit of 2.2×10^{-6} is placed on $\mathcal{B}(B^+ \rightarrow \bar{K}_0^{*0}(1430)K^+)$. From simulation and the branching fraction $\mathcal{B}(B^+ \rightarrow \bar{K}_0^{*0}(1430)K^+)$ as obtained above, we estimate—assuming zero interference—that $5_{-5}^{+14} B^+ \rightarrow \bar{K}_0^{*0}(1430)(\rightarrow K^-\pi^+)K^+$ events will be present in the region $0.744 < m_{K\pi} < 1.048 \text{ GeV}/c^2$, contributing 2_{-2}^{+6} events to the fitted $B^+ \rightarrow \bar{K}^{*0}(892)(\rightarrow K^-\pi^+)K^+$ signal yield. The central value of this estimated contribution is calculated from the central value of $\mathcal{B}(B^+ \rightarrow \bar{K}_0^{*0}(1430)K^+)$ while the uncertainty on the contribution covers the contribution obtained from the upper limit on $\mathcal{B}(B^+ \rightarrow \bar{K}_0^{*0}(1430)K^+)$ and uncertainties in the parameterization of the $\bar{K}_0^{*0}(1430)$ lineshape.

A correction is applied to the fitted $B^+ \rightarrow \bar{K}^{*0}(892)(\rightarrow K^-\pi^+)K^+$ yield to account for $B^+ \rightarrow \bar{K}_0^{*0}(1430)(\rightarrow K^-\pi^+)K^+$; including a component in the fit is ineffectual since $B^+ \rightarrow \bar{K}_0^{*0}(1430)(\rightarrow K^-\pi^+)K^+$ is signal-like in the majority of the fit variables.

An unbinned extended maximum likelihood fit to the five variables m_{ES} , ΔE , \mathcal{F} , $m_{K\pi}$, and $\cos\theta_H$, is used to extract the total number of $B^+ \rightarrow \bar{K}^{*0}(892)(\rightarrow K^-\pi^+)K^+$ and continuum background events. The likelihood for the selected sample is given by the product of the probability density functions (PDFs) for each indi-

TABLE I: PDFs are described by one or more of the following functions: ARGUS [17] (A), Breit-Wigner (BW), Crystal Ball [18] (CB), double Gaussian (DG), $\exp(P) + C$ —where P is a polynomial in the fit variable and C is a real scalar (E), Gaussian (G), linear (L), one-dimensional non-parametric [19] (N), quadratic (Q), Voigtian—a Gaussian convolved with a Breit-Wigner (V).

Component	PDF variable				
	m_{ES}	ΔE	\mathcal{F}	$m_{K\pi}$	$\cos\theta_H$
Signal					
Truth-matched	CB	DG	DG	BW	E
SCF	CB	L	DG	G+L	E
Background					
Continuum	A	L	DG	BW+L	Q
$B^+ \rightarrow \phi K^+$	CB	G+L	DG	V+E	E
$B^+ \rightarrow K^+ K^- K^+$	A+G	G+L	DG	Q	N
$B^+ \rightarrow \rho K^+$	CB	G+L	G	G+L	E

vidual candidate, multiplied by the Poisson factor:

$$\mathcal{L} = \frac{1}{N!} e^{-N'} (N')^N \prod_{i=1}^N \mathcal{P}_i, \quad (1)$$

where N and N' are the number of observed and expected events, respectively. The PDF \mathcal{P}_i for a given event i is the sum of the signal (S) and background (B) terms:

$$\mathcal{P}_i = N^S ((1-f)(\mathcal{P}^S)_i + f(\mathcal{P}_{SCF}^S)_i) + \sum_{j=1}^4 N_j^B (\mathcal{P}_j^B)_i, \quad (2)$$

where N^S and N_j^B are the yields for the signal component and the background components j , and $f = 0.06$ is the fraction of SCF signal events (treating true signal and SCF separately reduces the correlation between m_{ES} and $\cos\theta_H$ for signal from 14% to 1%). The four background terms comprise the continuum distribution and the three B meson background modes described above. The PDF for each component is the product of the PDFs for each of the fit input variables: $\mathcal{P} = \mathcal{P}_{m_{ES}} \mathcal{P}_{\Delta E} \mathcal{P}_{\mathcal{F}} \mathcal{P}_{m_{K\pi}} \mathcal{P}_{\cos\theta_H}$. Any correlations between the variables are such that biases brought about in the fit are negligible and we treat each PDF as independent and uncorrelated.

The PDF forms are presented in Table I. The parameters of the signal and B meson background PDFs are held fixed to the MC values. The parameters of the continuum PDFs are allowed to float except for the endpoint of the ARGUS function. The signal and continuum yields are floated in the fit while the three B meson background yields are fixed to their MC expectations.

Individual contributions to the systematic uncertainty are summarized in Table II. The systematic uncertainties that arise from fixing PDF parameters for the signal and B meson background components are estimated by varying these parameters, one at a time. Correlated parameters in the relevant PDF are adjusted accordingly and

the maximum likelihood fit is repeated with the shift in the signal yield taken to be the systematic uncertainty. The parameters are varied either by the 1σ uncertainties obtained when evaluating them from MC or such that we account for any discrepancy observed between data and MC (whichever is larger). Such discrepancies are identified with the calibration channel $B^+ \rightarrow \bar{D}^0 \pi^+$, which has a topology similar to the signal and a much higher branching fraction. For $\mathcal{P}_{\cos\theta_H}^S$, rather than varying the PDF parameters, a second-order polynomial is used. This is the expected shape when neglecting detector and reconstruction effects. For the non-parametric PDF, its smoothness is varied. The positive and negative shifts for each varied PDF parameter/shape are added separately in quadrature. The same procedure is used for the fixed yields of the B meson background modes and for the SCF fraction, f , which is varied by $\pm 20\%$ (relative). The uncertainty due to fixing the ARGUS endpoint for the continuum background m_{ES} PDF is found by floating this parameter and observing the shift in the signal yield; this shift is found to be less than a hundredth of an event. The systematic uncertainties associated with the subtraction of events from the fitted signal yield due to $B^+ \rightarrow \bar{K}_0^{*0}(1430)(\rightarrow K^- \pi^+) K^+$ and other non- $K^+ K^- \pi^+$ -final-state B meson decays have been discussed above.

The remaining systematic uncertainty on the signal yield is due to possible interference between final states. Several thousand MC datasets are produced each containing $B^+ \rightarrow \bar{K}_0^{*0}(892)(\rightarrow K^- \pi^+) K^+$ and $B^+ \rightarrow \bar{K}_0^{*0}(1430)(\rightarrow K^- \pi^+) K^+$ events that are generated according to their Breit-Wigner and LASS lineshapes, respectively. Interference between the two modes at the amplitude level is modeled. The relative magnitudes and phases of the two contributing amplitudes are varied randomly between datasets, but the numbers of events present in the regions $0.744 < m_{K\pi} < 1.048 \text{ GeV}/c^2$ and $1.048 < m_{K\pi} < 1.800 \text{ GeV}/c^2$ are the same for each dataset and are equal to the numbers we observe in data. The fractional systematic uncertainty is taken to be twice the standard deviation of the distribution of the fraction f_{892} divided by its average and is found to be 8%. For a generated dataset, f_{892} is the modulus squared of the amplitude of the $B^+ \rightarrow \bar{K}_0^{*0}(892)(\rightarrow K^- \pi^+) K^+$ mode integrated over the full Dalitz plot, divided by the modulus squared of the sum of the amplitudes of the $B^+ \rightarrow \bar{K}_0^{*0}(892)(\rightarrow K^- \pi^+) K^+$ and $B^+ \rightarrow \bar{K}_0^{*0}(1430)(\rightarrow K^- \pi^+) K^+$ modes integrated over the full Dalitz plot.

The uncertainties on reconstruction and selection criteria efficiencies are evaluated by comparing efficiencies for MC and data control samples. A systematic uncertainty of $\pm 1.4\%$ per track added linearly is taken for the particle identification efficiency. A systematic uncertainty of $\pm 0.8\%$ on the tracking efficiency is applied for each charged track, added linearly. The systematic uncertainty on the efficiency of the selection criteria is found to be $\pm 13\%$. The systematic uncertainty on the

TABLE II: Breakdown of systematic uncertainties.

Systematic effect	Uncertainty
Yield	
Fixed PDF parameters	+1.8 -1.1 events
Fixed SCF fraction	± 0.7 events
Fixed B meson background yields in fit	+0.4 -0.6 events
B meson background contribution	
Non- $K^+K^-\pi^+$ -final-state	± 3.2 events
$K^+K^-\pi^+$ -final-state	+2.0 -5.8 events
Final state interference	± 2.0 events
Reconstruction and selection criteria efficiency (RSC)	
Tracking	$\pm 2.4\%$
Particle identification	$\pm 4.2\%$
Selection criteria	$\pm 13.0\%$
Yield total	+4.7 -7.1 events
RSC total	$\pm 13.8\%$
Total number of B events	$\pm 1.1\%$
Total systematic uncertainty ($\times 10^{-6}$) on $\mathcal{B}(B^+ \rightarrow \bar{K}^{*0}(892)K^+)$	
	± 0.2

total number of B events is $\pm 1.1\%$.

A total of 38,690 events are fitted. The numbers of $B^+ \rightarrow \phi K^+$, $B^+ \rightarrow K^+K^-K^+$, and $B^+ \rightarrow \rho K^+$ events expected in this sample, estimated from simulation, are 21 ± 2 , 23 ± 2 , and 4 ± 1 , respectively. The yields for these B meson background components are fixed at the central values. The raw signal yield extracted from the fit is 30 ± 13 [stat] ± 3 [syst] events, of which 5_{-4}^{+7} [syst] are estimated to be B meson background events. The number of true signal events present in the on-resonance data sample is therefore 25 ± 13 [stat] ± 7 [syst]. The statistical significance of the result in the absence of systematic uncertainties, defined as the square root of the difference between the value of $-2 \ln \mathcal{L}$ for zero signal events and at its minimum, is 3.1σ . Accounting for systematic uncertainties, this significance is reduced to 1.6σ . The number of signal events is divided by the product of the signal efficiency and the total number of B events to give the branching fraction $\mathcal{B}(B^+ \rightarrow \bar{K}^{*0}(892)K^+) = (0.6 \pm 0.3$ [stat] ± 0.2 [syst]) $\times 10^{-6}$. Since the signal is not significant, we place an upper limit on this measurement at the 90% CL: $\mathcal{B}(B^+ \rightarrow \bar{K}^{*0}(892)K^+) < 1.1 \times 10^{-6}$. The likelihood function defined in Eq. (1) is modified to incorporate systematic uncertainties through convolution with a bifurcated Gaussian whose standard deviations are set to the (asymmetric) total systematic uncertainties described above. The 90% CL upper limit is then defined to be the value of the branching fraction $\mathcal{B}(B^+ \rightarrow \bar{K}^{*0}(892)K^+)$ (which corresponds to a particular value of N^S) below which lies 90% of the total integral of the modified likelihood function in the positive branch-

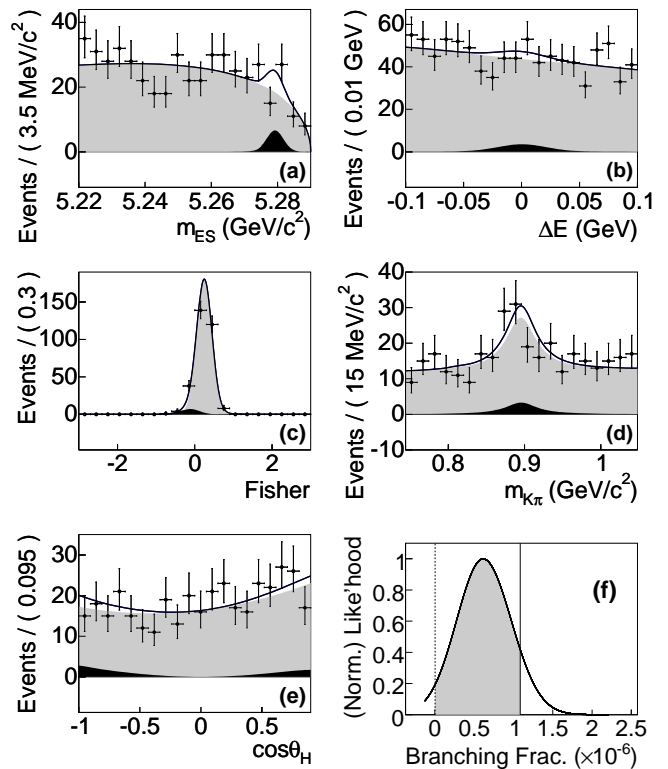


FIG. 1: (a)-(e): distributions of m_{ES} , ΔE , \mathcal{F} , $m_{K\pi}$, and $\cos\theta_H$. The points with uncertainties show the data. The curves show projections of the maximum likelihood fit. A selection requirement on the likelihood ratio has been applied as described in the text. The black, solid curve (no filling) shows the sum of all fitted components. The curve with gray filling shows the sum of all background components. The curve with black filling shows the signal component; (f): likelihood (modified to account for systematic uncertainties, and normalized) as a function of $\mathcal{B}(B^+ \rightarrow \bar{K}^{*0}(892)K^+)$. The shaded area represents 90% of the total area under the curve in the positive branching fraction region.

ing fraction region. This is illustrated in Fig. 1 (bottom row, right).

The results of the fit to $B^+ \rightarrow \bar{K}^{*0}(892)(\rightarrow K^-\pi^+)K^+$ are illustrated in Fig. 1. The plots are enhanced in signal by selecting only those events that exceed an optimized threshold for the likelihood ratio $R = N^S \mathcal{P}^S / (N^S \mathcal{P}^S + \sum_{j=1}^4 N_j^B \mathcal{P}_j^B)$ where N are the central values of the yields and \mathcal{P} are the PDFs with the projected variable integrated out.

In conclusion, we have reduced the 90% CL upper limit on the branching fraction for the decay $B^+ \rightarrow \bar{K}^{*0}(892)K^+$ from 5.3×10^{-6} [7] to 1.1×10^{-6} . The central value has been measured to be $(0.6 \pm 0.3$ [stat] ± 0.2 [syst]) $\times 10^{-6}$ with a significance of 1.6σ , consistent with the predictions of [2], [3], and [4]. This measurement can be used to determine an upper bound on $\Delta S_{\phi K_S^0}$. The technique described in Sec. VI of [1] is used, together with Eq. (29) of [5] and the findings of the $B^+ \rightarrow \phi\pi^+$

and $B^+ \rightarrow \phi K^+$ analyses described in [20] and [14, 21–23], respectively, to place a 90% CL upper bound of 0.11 on $|\Delta S_{\phi K_S^0}|$. Systematic uncertainties on the branching fractions used to determine this bound are accounted for. The bound presented here is significantly more restrictive than the bounds of ≈ 0.4 found in [1, 24]. We note that these latter bounds are based on fewer theoretical assumptions (see [5]). We have also placed an upper limit of 2.2×10^{-6} on the previously unmeasured branching fraction of the decay $B^+ \rightarrow \bar{K}_0^{*0}(1430)K^+$.

We are grateful for the excellent luminosity and ma-

chine conditions provided by our PEP-II colleagues, and for the substantial dedicated effort from the computing organizations that support *BABAR*. The collaborating institutions wish to thank SLAC for its support and kind hospitality. This work is supported by DOE and NSF (USA), NSERC (Canada), CEA and CNRS-IN2P3 (France), BMBF and DFG (Germany), INFN (Italy), FOM (The Netherlands), NFR (Norway), MIST (Russia), MEC (Spain), and STFC (United Kingdom). Individuals have received support from the Marie Curie EIF (European Union) and the A. P. Sloan Foundation.

-
- [1] B. Aubert et al. (*BABAR* Collaboration), Phys. Rev. **D74**, 072008 (2006).
 - [2] R. Fleischer and S. Recksiegel, Phys. Rev. **D71**, 051501 (2005) and PoS **HEP2005**, 255 (2006).
 - [3] C.-W. Chiang et al., Phys. Rev. **D69**, 034001 (2004).
 - [4] L. Guo et al., Phys. Rev. **D75**, 014019 (2007).
 - [5] Y. Grossman et al., Phys. Rev. **D68**, 015004 (2003).
 - [6] A. Soni and D. A. Suprun, Phys. Rev. **D75**, 054006 (2007).
 - [7] C. P. Jessop et al. (CLEO Collaboration), Phys. Rev. Lett. **85**, 2881 (2000).
 - [8] B. Aubert et al. (*BABAR* Collaboration), Nucl. Instrum. Meth. **A479**, 1 (2002).
 - [9] B. Aubert et al. (*BABAR* Collaboration), Phys. Rev. **D69**, 071101 (2004).
 - [10] D. J. Lange, Nucl. Instrum. Meth. **A462**, 152 (2001).
 - [11] S. Agostinelli et al. (GEANT4 Collaboration), Nucl. Instrum. Meth. **A506**, 250 (2003).
 - [12] B. Aubert et al. (*BABAR* Collaboration), Phys. Rev. **D72**, 072003 (2005).
 - [13] B. Aubert et al. (*BABAR* Collaboration), Phys. Rev. Lett. **89**, 201802 (2002).
 - [14] A. Garmash et al. (BELLE Collaboration), Phys. Rev. **D71**, 092003 (2005).
 - [15] D. Aston et al. (LASS Collaboration), Nucl. Phys. **B296**, 493 (1988).
 - [16] S. Eidelman et al. (Particle Data Group), Phys. Lett. **B592**, 1 (2004).
 - [17] H. Albrecht et al. (ARGUS Collaboration), Phys. Lett. **B241**, 278 (1990).
 - [18] M. J. Oreglia, Ph.D. thesis, SLAC-236 (1980), Appendix D; J. E. Gaiser, Ph.D. thesis, SLAC-255 (1982), Appendix F; T. Skwarnicki, Ph.D. thesis, DESY F31-86-02 (1986), Appendix E.
 - [19] K. S. Cranmer, Comput. Phys. Commun. **136**, 198 (2001).
 - [20] B. Aubert et al. (*BABAR* Collaboration), Phys. Rev. **D74**, 011102 (2006).
 - [21] B. Aubert et al. (*BABAR* Collaboration), Phys. Rev. **D74**, 032003 (2006).
 - [22] R. A. Briere et al. (CLEO Collaboration), Phys. Rev. Lett. **86**, 3718 (2001).
 - [23] D. Acosta et al. (CDF Collaboration), Phys. Rev. Lett. **95**, 031801 (2005).
 - [24] B. Aubert et al. (*BABAR* Collaboration), Phys. Rev. **D74**, 051106 (2006).